

Hydrothermal Liquefaction of Microalgae to Bio-oil Using Zeolite Catalysts

Anita Ramli^{a,b*}, Afeefah Fakhruddin^b, Adam Azmi^b, Nur Akila Syakida Idayu Khairul Anuar^b

^aHICoE Centre of Biofuel and Biochemical Research, Institute of Sustainable Energy & Resources, Universiti Teknologi PETRONAS, 32610 Seri Iskandar, Perak, Malaysia; ^bDepartment of Fundamental and Applied Sciences, Universiti Teknologi PETRONAS, 32610 Seri Iskandar, Perak, Malaysia

Abstract Mesoporous zeolite silica-alumina catalysts were investigated for their impact on the hydrothermal liquefaction (HTL) to convert *Nannochloropsis oculata* into bio-oil. The commercial catalysts were characterized using characterization instruments which are XRD, SAP, and TPD-NH₃ analysis, revealing distinctive structural and physicochemical properties. The catalytic screening was conducted at varied reaction temperatures (160–240 °C), durations (60–120 min), and catalyst loadings (1–5 wt.%). The result revealed that ZSM-5 demonstrates effectiveness as a catalyst for the HTL of *Nannochloropsis oculata*, yielding high bio-oil production under optimized conditions. Strong acid sites and high surface area density are highlighted as the key factors contributing to the catalyst's enhanced performance in promoting valuable bio-oil components.

Keywords: Zeolite catalysts, hydrothermal liquefaction (HTL), *Nannochloropsis oculata*, bio-oil.

Introduction

Fossil fuel combustion and industrial processes generated 256.05 million tonnes of carbon dioxide emissions in Malaysia in 2021. Until now, CO₂ has been the main contributor to greenhouse gases that cause the change of the climate of the earth. The sources of these gas emissions come from electricity production, which comes from burning fossil fuels, from agriculture, due to the release of methane from feedstocks such as biomass and transportation, due to the high energy consumption coming from fossil fuels, which when burned, causes the release of CO₂. In line with Malaysia's commitment to mitigating climate change, Malaysia's Ministry of Energy and Natural Resources (KeTSA) has set an ambitious target of achieving 31% renewable energy penetration in the country's installed electricity generation capacity by 2025. To achieve this goal a renewable energy policy framework was created, the Malaysia Renewable Energy Roadmap (MyRER). This roadmap objective aligns with Malaysia's broader pledge to reduce its economy-wide carbon intensity by 45% by 2030.

Biofuels hold promise as a viable replacement for current petroleum-based fuels, offering compatibility with existing transportation infrastructure and harnessing renewable energy for sustainability and greenhouse gas reduction. Third-generation biofuels derived from microalgae have emerged as a promising alternative. Microalgae can be cultivated and harvested in various conditions, possess CO₂ sequestration capabilities, and exhibit high lipid production [1]. Moreover, microalgae cultivation does not require direct sunlight; artificial light from lamps can be employed in laboratory settings. The harvested microalgae can then be processed to produce biofuels. Numerous conversion methods are used in microalgae-derived biofuel research, including pyrolysis, the Bligh and Dyer method, and Soxhlet extraction. In recent years, the implementation of hydrothermal liquefaction (HTL) as a conversion method has gained significant traction among researchers. HTL, a thermochemical conversion process, utilizes water, high temperature, and pressure conditions to transform wet biomass directly into liquid biofuels, eliminating the need for a preliminary drying step. This reduces energy consumption and simplifies the overall process, making HTL a promising approach for bio-oil production from microalgae [2].

*For correspondence:
anita_ramli@utp.edu.my

Received: 05 July 2024

Accepted: 24 Sept. 2024

©Copyright Ramli. This article is distributed under the terms of the [Creative Commons Attribution License](#), which permits unrestricted use and redistribution provided that the original author and source are credited.

While microalgae hold immense promise as a sustainable feedstock for bio-oil production, HTL faces significant challenges in achieving optimal bio-oil yield and minimizing byproduct formation. Past studies have highlighted two key issues that hinder the widespread adoption of HTL: the high cost of catalysts, particularly noble metal catalysts, and catalyst deactivation during the HTL process [3]. Both factors contribute to low yields and compromised bio-oil quality. Hence, current research efforts are focusing on identifying and developing alternative catalyst materials that are less expensive and more abundant than noble metals. One of the examples is zeolite catalysts, which have demonstrated potential in enhancing HTL performance [4]. However, their effectiveness and optimization strategies remain largely unexplored.

In this present study, we aim to evaluate the performance of commercial zeolite-based catalysts for hydrothermal liquefaction to convert *Nannochloropsis oculata* and optimize HTL process parameters, including temperature, reaction duration, and catalytic loading, to maximize bio-oil yield and quality. A comprehensive optimization study will be undertaken to identify the optimal operating parameters that maximize conversion efficiency and bio-oil yield.

Materials and Methods

Materials

Commercial zeolite was purchased from ACS Materials, Inc. The chosen zeolites are ZSM-5, SAPO-34, and Al-MCM-41. Table 1 below showing the Si:Al ratio of each catalyst. This ratio represents the molar ratio of silicon (Si) to aluminum (Al) in the zeolite framework. *Nannochloropsis oculata* microalgae were obtained from Laboratory & Scientific Enterprise as the feedstock for hydrothermal liquefaction.

Table 1. Si:Al ratio of zeolite catalysts

Type of zeolite	Si:Al ratio
ZSM-5	38
SAPO-34	0.5
Al-MCM-41	25

Catalyst Characterization

The zeolite crystalline structure of the catalysts was verified using X-ray diffraction recorded by Panalytical model Xpert3 Powder. The scanning parameters were set to a step size of 0.05° and a dwell time of 2 seconds per step, with 2θ angles ranging from 5 to 45° for ZSM-5, 5 to 50° for SAPO-34, and 1 to 10° for Al-MCM-41. The textural properties of the catalysts, including surface area, average pore size, and pore volume, were determined using Micromeritics model ASAP2020. Prior to analysis, all catalysts underwent a degassing process under vacuum at 250 °C for 240 minutes. The Brunauer-Emmett-Teller (BET) and Barret-Joyner-Halenda (BJH) methods were employed to calculate the catalysts' total surface area and pore size distribution respectively. Catalytic acidity was assessed using temperature-programmed desorption (TPD) employing ammonia as the probe molecule (Thermo model TPDRO 1100). In the initial step, samples were pre-treated in a helium gas flow of 20 ml/min at 500 °C for 30 minutes. Subsequently, ammonia adsorption was conducted at 30 °C for 30 minutes. Finally, the catalysts were subjected to a temperature ramp from 30 °C to 600 °C at a heating rate of 10°C/min.

Hydrothermal Liquefaction of *Nannochloropsis Oculata*

The catalytic performance of all zeolite catalysts was assessed through HTL using a high-pressure autoclave reactor to convert *Nannochloropsis oculata* microalgae into bio-oil. The reactor was charged with 10 g of the microalgae, 100 ml of distilled water, and 0.5 g of the catalyst (5 wt.% relatives to the microalgae). The mixture was stirred, heated to 240 °C, and held for 1 hour. The reactor was left to cool to room temperature, and the reaction products were collected and filtered from solid residues. Then the liquid product was subsequently air dried to remove water residual. The final product, which was a dark viscous liquid was obtained. All catalysts were calcined at 550 °C for 2 hours prior to HTL. The experiments were replicated three times with different zeolite catalysts and also blank run as a control parameter. Catalysts with the highest bio-oil yield and conversion will be used to study the effect of HTL reaction parameter. The optimized HTL process was acquired for various reaction temperatures (160, 200, and 240 °C), duration (60, 90, and 120 min), and catalyst loading (1, 3, and 5 wt.%). The yield of various fractions will be calculated by using various equations are provided below.

$$\text{Conversion (\%)} = \frac{\text{Weight of feed} - \text{solid residue}}{\text{Weight of feedstock}} \times 100$$

$$\text{Bio-oil yield (\%)} = \frac{\text{Weight of bio-oil}}{\text{Weight of feedstock}} \times 100$$

$$\text{Solid residue yield (\%)} = \frac{\text{Weight of solid residue}}{\text{Weight of feedstock}} \times 100$$

Characterization of Bio-Oil

Qualitative analysis of bio-oil produced by the best catalyst was performed using GC–MS (Shimadzu GCMS- QP2020), which is equipped with a DB-5 ms column (30 m × 250 μm × 0.25 μm). The initial oven temperature was set at 50 °C for 2 min, then was ramped to 120 °C at a rate of 10 °C/min, followed by rising up to 280 °C at 8 °C/min and finally kept at 280 °C for 5 min. Helium gas was used as the carrier gas with a total flow rate of 40 mL/min. To conduct a qualitative analysis of degradation products, the NIST MS database version 2.2 (2014) library was employed.

Results and Discussion

Physicochemical Properties of the Catalysts

X-ray diffractogram pattern of all zeolites illustrated in Figure 1 reveals the distinct peaks of each zeolite species. Figure 1(a) shows the XRD pattern for ZSM-5 with distinct peaks at 2θ = 7-9° and 23-25°, indicative of its orthorhombic structure (ICDD 98-006-8256). While in Figure 1(b) shows the XRD pattern for SAPO-34 by exhibiting sharp and well-defined diffraction peaks at 9.58°, 13.02°, 16.17°, 17.85°, 20.82°, 25.05°, 26.21°, and 30.93° which is aligned with the hexagonal structure (ICDD 98-009- 0140). Figure 1(c) presents the XRD pattern for Al-MCM-41 formed a single broad peak at 2θ = 4.09°, featuring as amorphous aluminosilicate with a highly ordered hexagonal structures (ICDD 98-008-7510).

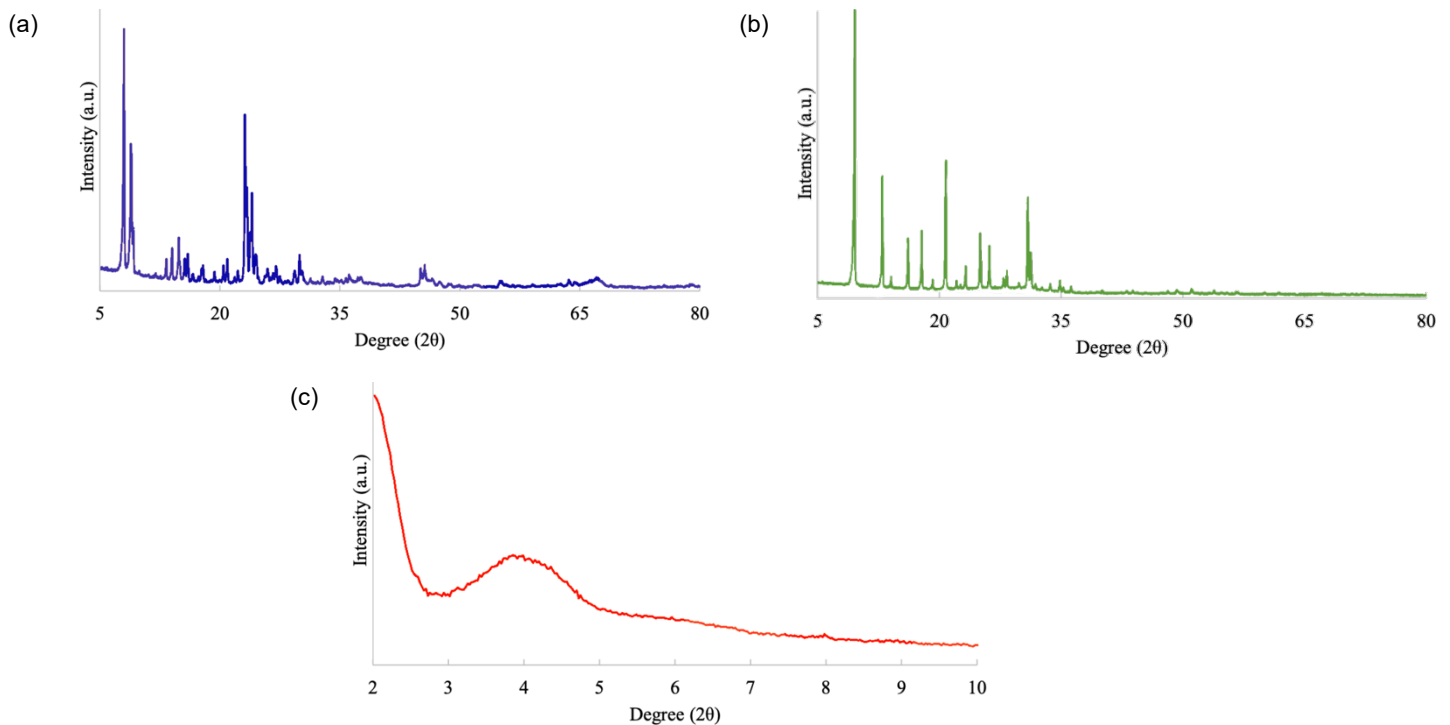


Figure 1. XRD patterns for (a) ZSM-5, (b) SAPO-34, (c) Al-MCM-41

Work done by Da Silva *et al.* [5] stated the same intense peak was observed at 7-9° and 23-25° for hydrothermal synthesis of ZSM-5 zeolite. The observed diffraction patterns of SAPO-34 are aligned with the findings of Aldeen *et al.* [6], which reported identical diffraction peaks for the commercial SAPO-34.

The pattern observed in Al-MCM-41 aligns with the findings of Chang *et al.* [7], who obtained a similar diffractogram for meso-structured Al-MCM-41 material impregnated with bromocresol green (BG) dye. Cross-referencing the XRD patterns obtained in this study with those reported in the literature served to validate the structure of the synthesized catalyst.

The crystallite sizes of the catalysts were calculated using the Debye-Scherrer Equation, as summarized in Table 2. Generally, larger crystallites demonstrate improved stability and reduced deactivation, whereas smaller crystallites often provide enhanced surface area and accessibility. As observed in the X-ray diffractogram in Figure 1, SAPO-34 exhibits the largest crystallite size (113.9 nm), which is attributed to the formation of distinct and intense peaks. ZSM-5 also possesses a relatively large crystallite size (85.5 nm), which is evident from the sharp and high-intensity peaks. In contrast, Al-MCM-41 has the smallest crystallite size (12.7 nm) due to its broad peaks.

Table 2. Physicochemical properties and acidities of different catalysts

Catalyst	Surface area (m ² /g)	Pore Volume (m ³ /g)	Pore Size (nm)	Crystallite Size (nm)
ZSM-5	285	182.9	5.09	85.5
SAPO-34	515	0.044	70.5	113.9
Al-MCM-41	719	893.0	3.45	12.7

The surface area, pore size, and pore volume are summarized in Table 2. Among the three zeolites studied, Al-MCM-41 exhibited the largest surface area (719 m²/g), followed by SAPO-34 with 514.9 m²/g. The finer structure of Al-MCM-41 leads to smaller particle sizes have contributed to its large surface area, as demonstrated by Huo *et al.* [3]. In contrast, ZSM-5, with the smallest surface area (285 m²/g), was manually ground due to its initial form as pallets. This manual grinding process may have prevented ZSM-5 from achieving the same level of structural finesse as the other two zeolites.

Despite having the lowest total pore volume (0.044 m³/g), SAPO-34 possessed the highest average pore size of 70.5 nm. This is very contradictory with ZSM-5 and Al-MCM-41 because despite having smaller average pore sizes (5.09 nm for ZSM-5 and 3.45 nm for Al-MCM-41), they both exhibit a larger total pore volume (182.9 m³/g and 893 m³/g respectively). These structural characteristics may influence the catalytic performance of these materials during microalgae conversion to bio-oil.

N₂ adsorption-desorption isotherm of all zeolite catalysts are depicted in Figure 2. Isotherm for ZSM-5 zeolite catalyst (Figure 2(a)) reveals a unique combination of Type I and Type IV(a) characteristics, accompanied by a subtle H2(b) hysteresis loop in the P/P° range of 0.5-0.9. This intriguing profile suggests the coexistence of narrow micropores and ordered mesopores within the zeolite's structure, hinting at a potential pore-blocking mechanism. While in Figure 2(b), the isotherm of SAPO-34 zeolite exhibits a Type I isotherm, characterized by a sharp increase in adsorption at relative pressures close to zero. This observation is indicative of the presence of micropores within the zeolite structure. On the other hand, Al-MCM-41 material exhibited a Type IV(b) isotherm with a distinct H1-type hysteresis loop, as illustrated in Figure 2(c). The observation can be attributed to the well-organized mesoporous structure and the consistent distribution of pore sizes within the catalyst framework.

The trait observed in Figure 2(a) is in agreement with Rutkowska *et al.* [8], who verified the presence of both micro and mesopores in their synthesized zeolites by observing increased adsorption at relative pressures (P/P°) < 0.05 and the appearance of a hysteresis loop in the P/P° range of 0.4 to 0.9, characteristics typically associated with Type I and Type IV adsorption isotherms, respectively. The hysteresis loop observed in the N₂ adsorption-desorption isotherm suggests capillary condensation within the mesopores of the ZSM-5 zeolite. When the relative pressure is decreased, desorption does not occur immediately, resulting in a hysteresis loop [9].

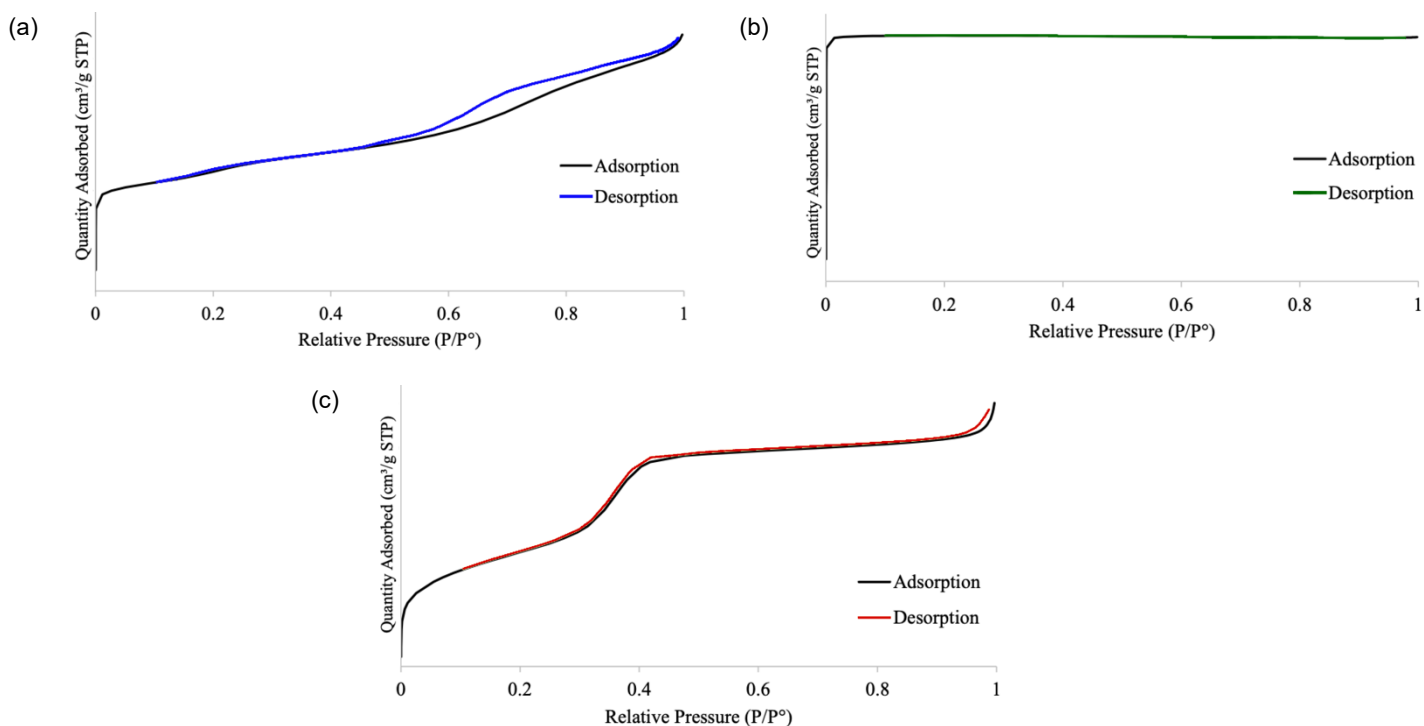


Figure 2. Isotherm plotline for (a) ZSM-5, (b) SAPO-34, (c) Al-MCM-41

This finding obtained for SAPO-34 is consistent with the study conducted by Li *et al.* [10], who reported that the prepared SAPO-34/ZSM-5 composite also exhibited a Type I isotherm. However, the present study on SAPO-34 isotherm did not demonstrate any hysteresis loop, implying that the adsorption and desorption processes are reversible, with no significant energy barriers hindering the movement of adsorbate molecules between the adsorbent surface and the gas phase. This observation contrasts with the findings of Numpilai T. *et al.* [11], who reported the presence of a hysteresis loop for $\text{In}_2\text{O}_3/\text{SAPO-34}$ composite catalyst at around relative pressure 0.7-1.0 P/P° and a small hysteresis loop for SAPO-34 at around 0.8 P/P° . This contradiction might be due to different catalysts used in the two studies having different pore structures or surface properties, which could affect the adsorption and desorption behaviour of N_2 molecules. Further investigation is needed to determine the specific factors responsible for the absence of a hysteresis loop in the present study.

The discovery is consistent with the findings reported by Huo *et al.* [3] for highly ordered aluminium-containing mesoporous silica (Al-MCM-41) which state that during the adsorption process, the amount of adsorbed material gradually increased with rising relative pressure, primarily due to the formation of multiple adsorbate layers. A small hysteresis loop was observed at relative pressures between 0.25 and 0.4. Interestingly, no clear hysteresis loop was present above a relative pressure of 0.9; however, a distinct and sudden increase in adsorption was evident at relative pressures between 0.25 and 0.4 in the isotherm of the calcined sample. This increase can be attributed to the well-organized mesoporous structure and the sample's consistent distribution of pore sizes. Nugraha *et al.* [12] also reported similar findings for the isotherm pattern of modified Al-MCM-41 with NiO nanoparticles.

Acidic Properties of Catalysts

The acidity characteristics of the zeolite catalysts were determined by TPD analysis using ammonia. This analysis provides valuable insights into the total number, strength, and distribution of acid sites on the catalysts. Figure 3 shows the NH_3 -TPD pattern of ZSM-5, SAPO-34, and Al-MCM-41. The NH_3 -TPD patterns of ZSM-5 and SAPO-34 reveal distinct desorption peaks at around 450 and 550 °C (435 and 586 °C for ZSM-5, and 449 and 586 °C for SAPO-34), indicative of strong acid sites. Additionally, moderate acid sites are evident in a broad desorption peak ranging from 210-230 °C (212 °C for ZSM-5, and 225 °C for SAPO-34). Weak acid sites are present in a low-intensity peak at slightly above 100 °C. In contrast, Al-MCM-41 exhibits two prominent peaks at approximately 510 °C and 577 °C, confirming the presence of strong acid sites.

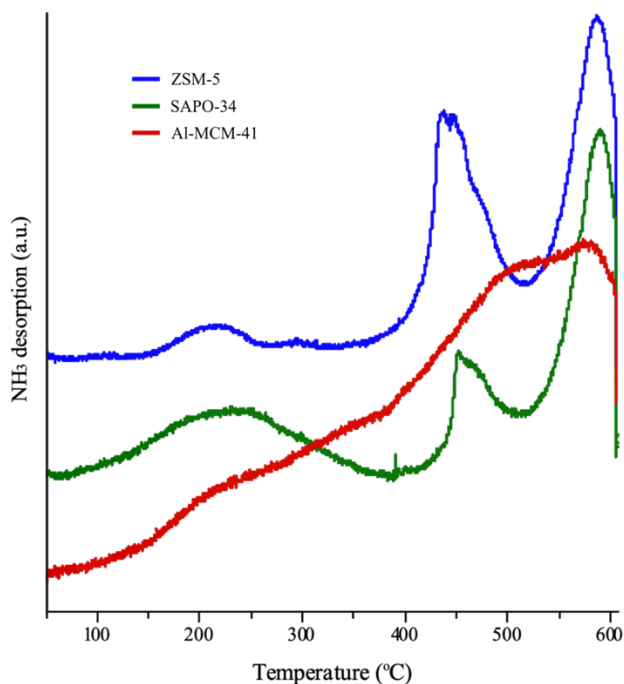


Figure 3. NH₃-TPD analysis for all zeolites

The lack presence of a weak acid site in ZSM-5 is caused by the NH₃ that is poorly coordinated and physisorbed on Lewis acid sites, while for the strong acid site, the NH₄⁺ ions containing three hydrogen atoms are bonded to three oxygen ions of AlO₄ tetrahedra on Brønsted acid sites [13]. Meanwhile, for SAPO-34, the desorption of NH₃ on the weak acid sites is caused by either Al-OH, Si-OH, or P-OH bonds, and the hydroxyl group (Si-OH-Al) causes the desorption on the strong acid sites [14]. Al-MCM-41 exhibits a high concentration of acid sites, primarily attributed to the formation of bridging Si(OH)Al groups that generate Brønsted acid sites through the isomorphous substitution of Si with Al. Simultaneously, Lewis acid sites arise from the coordinatively unsaturated Al³⁺ cations. This observation is corroborated by Venezia *et al.* [15], who investigated the impact of alumina content on the acidity of siliceous MCM-41. Their findings revealed that the number of sites available for NH₃ chemisorption increases alongside the alumina percentage in hybrid (x)Al/MCM-41 materials.

Table 3. Acid site density of zeolite catalyst

Catalyst	Acid sites (μmol/g)		Acid Site Density (μmol / m ³)
	Moderate	Strong	
ZSM-5	34.41	608.25	2.26
SAPO-34	35.84	243.81	0.54
Al-MCM-41	81.72	619.90	0.98

Table 3 presents the total acidity calculated from peak areas of all zeolites. As observed, strong acid sites dominate the distribution, indicating higher acidity. The total acidities of zeolite catalysts decreased in the following order: Al- MCM-41 > ZSM-5 > SAPO-34. In contrast to previous studies, the distribution of acid sites in the present study exhibits notable differences, particularly for ZSM-5 and SAPO-34. Yuan *et al.* [16] investigated the characteristics of ZSM-5 zeolites and reported higher peaks for weak acid sites compared to strong acid sites. Similarly, Ma *et al.* [17] studied metal-loaded ZSM-5 coupled with copper-zinc oxide and observed a similar pattern of acid site distribution in unmodified H-ZSM-5. For SAPO-34, a predominance of weak acid sites can be observed on Cu-SAPO-34 catalysts [18].

Catalytic Activities

Effect of Types of Catalyst

The types of catalyst will influence the product distribution from any catalytic reaction. Figure 4 shows the change in liquid yield by using blank and the three zeolite catalysts with fixed autogenous pressure. It was observed that the maximum bio-oil yield (59.2 wt%) was obtained by using ZSM-5 as the catalyst. Meanwhile, 58.0 wt% and 51.7 wt% bio-fuel yield was found for Al-MCM-41 and blank, respectively. SAPO-34 provides the lowest yield, with 48.5 wt%.

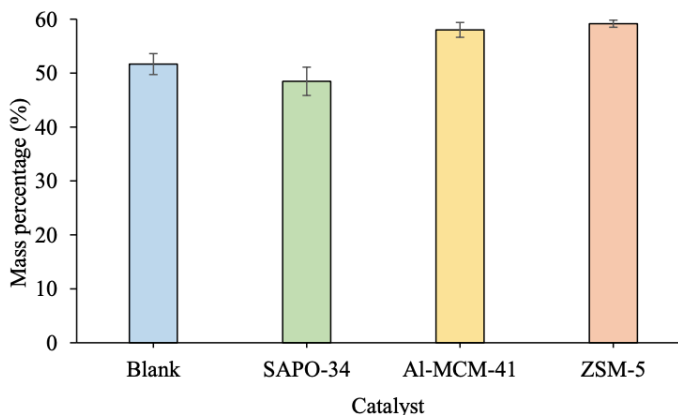


Figure 4. Effect of types of catalyst on bio-oil yield

Duan and Savage [19] reported that crude bio-oil yields from *Nannochloropsis* sp. ranged from 35% for uncatalyzed liquefaction to 57% for Pd/C-catalyzed liquefaction. The bio-oil yield can be correlated with the characteristics of the catalyst itself. Based on XRD results, ZSM-5 and Al-MCM-41 exhibit an orthorhombic structure, which may contribute to the increased bio-oil yield. This is likely due to their well-defined system of channels and pores of specific dimensions, which enables shape-selective catalysis. This allows for the selective conversion of certain biomass-derived compounds into bio-oil components while minimizing byproducts. Compared to the orthorhombic structure of ZSM-5 and Al-MCM-41, the hexagonal structure of SAPO-34 may be slightly less favorable for the conversion of microalgae biomasses.

Meanwhile, results from SAP analysis state that ZSM-5 and Al-MCM-41 have smaller average pore sizes than SAPO-34 but larger total pore volumes. This is likely because ZSM-5 and Al-MCM-41 have a more uniform distribution of pore sizes, while SAPO-34 has a wider range of pore sizes. The uniform distribution of pore sizes in ZSM-5 and Al-MCM-41 may make them more effective catalysts for converting microalgae to bio-oil, as this process requires the diffusion of reactants and products through the catalyst pores. Analysis of the catalysts using temperature-programmed desorption of ammonia (TPD-NH₃) revealed that ZSM-5 exhibited the highest acid site density (2.258 μmol/m²), while both ZSM-5 and Al-MCM-41 demonstrated a high concentration of strong acid sites. This enhanced acidity facilitated the efficient breakdown of macroalgae macromolecules into desired products [20]. In a prior study by Wang *et al.* [21] on catalytic HTL of *Spirulina*, NiO/SAPO-34 exhibited the highest bio-oil yield (59.85 wt.%) among the investigated different catalysts supports due to its superior acid site density, demonstrating the crucial role of acid sites in achieving high biofuel yields.

However, SAPO-34 has a lower liquid yield compared to the blank might be due to lack of strong acid site to allow more conversion to take place and SAPO-34 produce more gaseous product (higher in gaseous yield) compared to other catalyst used in several finding by Zhang *et. al* [22] & Kotelev *et. al* [23]. Furthermore, SAPO-34 has special water absorbing capacity which make SAPO-34 structure prone to hydrolyze resulting in lower conversion compared to the blank. This special ability led to the degradation of SAPO-34 structure as Si-O-Al bond hydrolyze by water and form Si-OH and Al-OH [24,25].

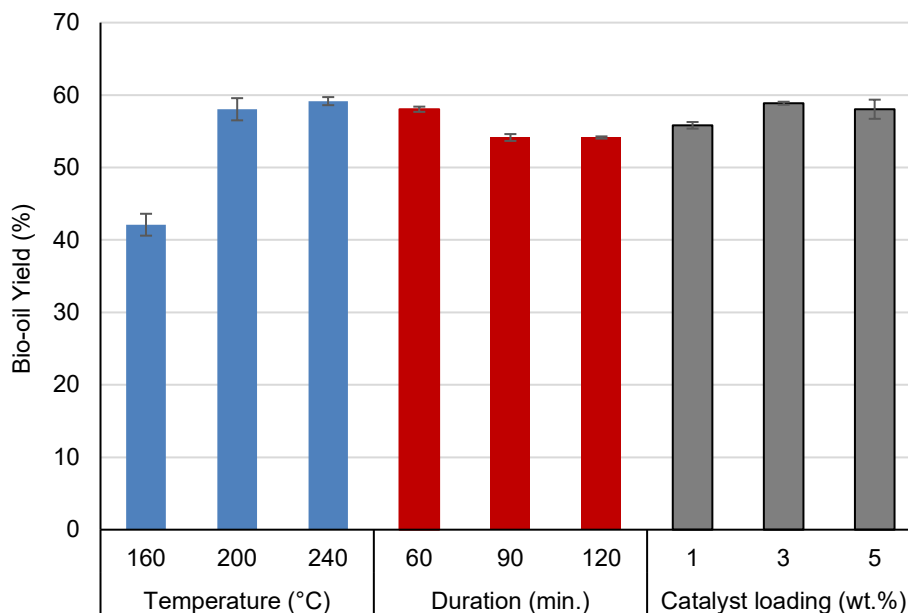
Table 4 below shows the bio-oil, solid residue, and conversion yield. As we can see, ZSM-5 produces the highest conversion rate at 77.61% and the lowest solid residue formation at 29.25%. This is attributed to the degradation of smaller liquid segments into non-condensable gases [26]. This phenomenon is further enhanced by secondary bio-oil cracking on the charcoal surface when exposed to elevated temperatures [27].

Table 4. Catalytic performance of *Nannochloropsis oculata* hydrothermal liquefaction over zeolites catalysts

Catalyst	Bio-oil (%)	Solid Residue (%)	Conversion (%)
Blank	51.67	29.25	70.75
SAPO-34	48.48	37.50	62.50
Al-MCM-41	58.01	34.46	65.54
ZSM-5	59.16	22.39	77.61

Effect of Reaction Parameters

Based on catalyst screening, ZSM-5 gives rise to the highest conversion and bio-oil yield. Therefore, for the study on the effect of reaction parameter, ZSM-5 was used to determine the effect of reaction temperature, duration, and catalyst loading. The different reaction temperatures (160, 200, and 240 °C), duration (60, 90, and 120 min), and catalyst loading (1, 3, and 5 wt.%) were applied for the optimization of HTL of *Nannochloropsis oculata*. The overall result of HTL yields is provided in Table A.1 while the comparison of bio-oil yield obtained is depicted in Figure 5.

**Figure 5.** Bio-oil yield obtained at different HTL conditions

An investigation into the effect of temperature on bio-oil production revealed a positive correlation between temperature and bio-oil yield. The maximum bio-oil yield of 59.16% was achieved at 240 °C. This enhancement in bio-oil yield can be attributed to the increased kinetic energy at higher temperatures, which facilitates the breakdown of chemical bonds in biomass. Li *et al.* [27] suggested that the repolymerization of active intermediate monomers of microalgae biomass further contributes to the increased bio-oil yield. Elevated temperatures also promote the cleavage of chemical bonds within the biomass, leading to subsequent hydrolysis and repolymerization reactions. These reactions resulted in bio-oil formation due to the formation of water-soluble products [28, 29]. In contrast, lower bio-oil yields were obtained at lower temperatures (160 °C) due to insufficient kinetic energy for the complete breakdown of biomass components from the microalgae. As a result, a significant amount of unreacted feedstock remains within the reactor rather than being converted into biochar.

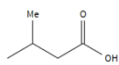
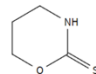
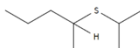
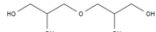
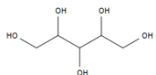
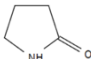
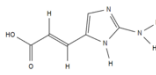
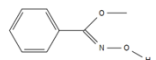
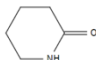
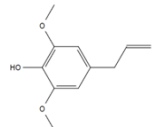
The data from the graph in Figure 5 on reaction duration reveals that as the reaction time increases, there is a corresponding decrease in the bio-oil yield, going from 58.04% at 60 minutes to 54.14% at 90 minutes. The reason for this decline is that prolonged reaction times lead to the decomposition of bio-oil and result in higher yields of gas and solid residue, as documented in the work of Li *et al.* [30].

Referring to Figure 5 on the catalyst loading, bio-oil yield slightly increases with increasing catalyst loading from 1 wt.% to 3 wt.%. Therefore, catalyst loading does not have significant impact on yield of bio-oil from the HTL of *Nannochloropsis oculata* using ZSM-5 as catalyst. The slight increase in bio-oil yield when catalyst loading is increased can be attributed to the presence of more active sites and the enhancement of collision frequency between catalyst and reactants. As the catalyst loading increases, more active sites become available to participate in the reaction, leading to a higher conversion of microalgae into bio-oil components. Additionally, the increased mass of the catalyst enhances the likelihood of collisions between catalyst molecules and reactants, resulting in faster reaction rates and higher bio-oil production. However, upon exceeding a certain threshold, the bio-oil yield reaches a point of stagnation and exhibits a slight decrease. This is evident in the case of elevating the catalyst mass to 5 wt.%, where the bio-oil yield experiences a marginal decline, reaching 58.04%. This observed reduction is likely attributed to the secondary cracking of bio-oil, a phenomenon associated with an excessive catalyst quantity [31].

Chemical Composition of Bio-Oil

GC chromatograms were employed to identify the presence of various composition products resulting from the conversion of *Nannochloropsis oculata* into liquid bio-oil. The profiles were matched with entries from the NIST14.L library. Figure A.2 illustrates the composition of bio-oil when the ZSM-5 catalyst was used, and Figure A.3 shows the bio-oil composition without any catalyst (blank).

Table 5. Composition of compound in bio-oil obtained

No.	Catalyst	Carbon Number	Retention Time (min.)	Area (%)		Chemical Structure
				ZSM-5	Blank	
1.	3-methylbutanoic acid	5	4.085	0.42	1.90	
2.	Tetrahydro-1, 3-oxazine-2-thione	4	6.081	6.12	2.97	
3.	2-(Isopropylsulfanyl)	5	6.339	19.59	52.96	
4.	Diglycerol	6	6.508	1.39	-	
5.	Xylitol	5	6.565	1.94	-	
6.	2-Pyrrolidinone	4	8.010	3.28	8.66	
7.	Imidazole, 2-amino-5-[(2-carboxy) vinyl]-	6	8.790	1.53	5.19	
8.	Methyl N-hydroxybenzimidate	8	9.027	1.83	2.51	
9.	2-Piperidinone	5	9.861	2.31	5.26	
10.	2,6-dimethoxy-4-(2-propenyl) phenol	11	13.212	1.36	-	

The composition of bio-oil obtained from catalyst screening for liquefaction (Table 5) revealed a diverse array of compounds. These compounds represent a wide spectrum of functional groups, encompassing carboxylic acids, heterocyclic compounds, cyclic amides, amino acids, carboxamides, alcohols, and aromatics, with thioether having the highest percentage with 19.59%, representing 2-(isopropylsulfanyl)pentane. The blank reaction yielded similar compounds but with varying area percentages. Notably, diglycerol and xylitol, were present in the ZSM-5-catalyzed reaction with area percentages of 1.39% and 1.94%, respectively, were absent in the blank. Comparing the compound abundances in chromatograms obtained from liquefaction reactions with and without a catalyst revealed a significant increase in abundance when the catalyst was employed.

In general, the hydrolysis of biomass constituents, including lipids, proteins, and carbohydrates, leads to the formation of active macromolecular compounds such as amino acids, fatty acids, and monosaccharides [32]. Hence, despite these similarities, there are also notable differences, particularly when compared to other studies. For instance, Ma *et al.* [20] reported the presence of hydrocarbon compounds such as undecane, 1-pentadecene, and benzaldehyde in bio-oil. Paper from Saber *et al.* [33] also reveals the presence of different components such as palmitic acid, phytol acetate, and pyrrolidine derivatives when liquefaction on *Nannochloropsis* sp.

Conclusions

Commercial ZSM-5 emerged as the optimal catalyst for microalgae liquefaction, producing the highest bio-oil yield of 59.16% at 77.61% conversion at 240 °C, 60 min, and 5 wt.% catalyst loading. GC-MS analysis revealed that the bio-oil compositions obtained with and without ZSM-5 were largely similar, with 2-(isopropylsulfanyl)pentane being the most abundant compound in both cases (19.59% for ZSM-5 and 52.96% for blank). The absence of diglycerol and xylitol in the bio-oil produced without ZSM-5, suggests that the catalyst plays a role in promoting the formation of these valuable products.

Conflicts of Interest

The author(s) declare(s) that there is no conflict of interest regarding the publication of this paper.

Acknowledgement

This research was funded by the Malaysian Ministry of Higher Education under the Yayasan Universiti Teknologi PETRONAS Grant Scheme (YUTP, cost centre 015LC0-386).

References

- [1] Sharara, M. A., Clausen, E. C., Carrier, D. J., Bergeron, C., & Ramaswamy, S. (2012). An overview of biorefinery technology. *Biorefinery Co-Products*, 1–18. <https://doi.org/10.1002/9780470976692.ch1>
- [2] Costa, P. A., Mata, R. M., Pinto, M. F., Paradela, F., & Dutra, F. (2022). Hydrothermal liquefaction of microalgae for the production of biocrude and value-added chemicals. *Chemical Engineering Transactions*, 94, 865–870. <https://doi.org/10.3303/CET2294144>
- [3] Huo, C., Ouyang, J., & Yang, H. (2014). CuO nanoparticles encapsulated inside Al-MCM-41 mesoporous materials via direct synthetic route. *Sci Rep*, 4, 3682. <https://doi.org/10.1038/srep03682>
- [4] Wang, W., Xu, Y., Wang, X., Zhang, B., Tian, W., Zhang, J. (2018). Hydrothermal liquefaction of microalgae over transition metal supported TiO₂ catalyst. *Bioresour. Technol.*, 250, 474–480. <https://doi.org/10.1016/j.biortech.2017.11.051>
- [5] Da Silva, V. J., Crispim, A. C., Queiróz, M. B., Menezes, R. R., Laborde, H. M., & Rodrigues, M. G. F. (2010). Structural and morphology characterization of ZSM-5 zeolite by hydrothermal synthesis. *Materials Science Forum*, 660–661, 543–548. <https://doi.org/10.4028/www.scientific.net/msf.660-661.543>
- [6] Aldeen, O. D. A. S., Mahmoud, M. Z., Majdi, H. S., Mutlak, D. A., Uktamov, K. F., & Kianfar, E. (2022). Investigation of effective parameters Ce and Zr in the synthesis of H-ZSM-5 and SAPO-34 on the production of light olefins from naphtha. *Advances in Materials Science and Engineering*, 2022, 1–22. <https://doi.org/10.1155/2022/6165180>
- [7] Chang, Y. C., Bai, H., Li, S. N., & Kuo, C. N. (2011). Bromocresol green/mesoporous silica adsorbent for ammonia gas sensing via an optical sensing instrument. *Sensors*, 11(4), 4060–4072. <https://doi.org/10.3390/s110404060>
- [8] Rutkowska, M., Macina, D., Piwowarska, Z., Gajewska, M., Díaz, U., & Chmielarz, L. (2016). Hierarchically structured ZSM-5 obtained by optimized mesotemplate-free method as active catalyst for methanol to DME conversion. *Catalysis Science & Technology*, 6(13), 4849–4862. <https://doi.org/10.1039/c6cy00040a>
- [9] Gregg, S. J., & Sing, K. S. W. (1982). Adsorption, surface area and porosity. *Berichte der Bunsengesellschaft*

- für Phys. Chemie*, 86(10), 957–957. <https://doi.org/10.1002/bbpc.19820861019>
- [10] Li, X., Rezaei, F., Ludlow, D. K., & Rownaghi, A. A. (2018). Synthesis of SAPO-34@ZSM-5 and SAPO-34@Silicalite-1 core-shell zeolite composites for ethanol dehydration. *Industrial & Engineering Chemistry Research*, 57(5), 1446–1453. <https://doi.org/10.1021/acs.iecr.7b05075>
- [11] Numpilai, T., Kahadit, S., Wittoon, T., Ayodele, B. V., Cheng, C. K., Siri-Nguan, N., Sornchamni, T., Wattanakit, C., Chareonpanich, M., & Limtrakul, J. (2021). CO₂ hydrogenation to light olefins over IN₂O₃/SAPO-34 and Fe-CO/K-Al₂O₃ composite catalyst. *Topics in Catalysis*, 64(5–6), 316–327. <https://doi.org/10.1007/s11244-021-01412-5>
- [12] Nugraha, R. E., Prasetyoko, D., Bahruji, H., Suprpto, S., Asikin-Mijan, N., Oetami, T. P., Jalil, A. A., Vo, D. N., & Taufiq-Yap, Y. H. (2021). Lewis's acid Ni/Al-MCM-41 catalysts for H₂-free deoxygenation of Reutealis trisperma oil to biofuels. *RSC Adv.*, 11(36), 21885–21896. <https://doi.org/10.1039/d1ra03145g>
- [13] Kalamaras, C. M., Palomas, D., Bos, A., Horton, A. D., Crimmin, M. R., & Hellgardt, K. (2016). Selective oxidation of methane to methanol over Cu- and Fe-exchanged zeolites: The effect of Si/Al molar ratio. *Catalysis Letters*, 146(2), 483–492. <https://doi.org/10.1007/s10562-015-1664-7>
- [14] Wang, Q., Zhang, W., Ma, X., Liu, Y., Zhang, L., Zheng, J., Wang, Y., Li, W., Fan, B., & Li, R. (2023). A highly efficient SAPO-34 catalyst for improving light olefins in methanol conversion: Insight into the role of hierarchical porosities and tailoring acid properties based on in situ NH₃-poisoning. *Fuel*, 331, 125935. <https://doi.org/10.1016/j.fuel.2022.125935>
- [15] Venezia, A. M., Murania, R., La Parola, V., Pawelec, B., & Fierro, J. (2010). Post-synthesis alumination of MCM-41: Effect of the acidity on the HDS activity of supported Pd catalysts. *Applied Catalysis A: General*, 383(1–2), 211–216. <https://doi.org/10.1016/j.apcata.2010.06.001>
- [16] Yuan, E., Han, W., Zhang, G., Zhao, K., Mo, Z., Lü, G., & Tang, Z. (2016). Structural and textural characteristics of Zn-containing ZSM-5 zeolites and application for the selective catalytic reduction of NO_x with NH₃ at high temperatures. *Catalysis Surveys from Asia*, 20(1), 41–52. <https://doi.org/10.1007/s10563-015-9205-3>
- [17] Ma, T., Imai, H., Yamawaki, M., Terasaka, K., & Li, X. (2014). Selective synthesis of gasoline-ranged hydrocarbons from syngas over hybrid catalyst consisting of metal-loaded ZSM-5 coupled with copper-zinc oxide. *Catalysts*, 4(2), 116–128. <https://doi.org/10.3390/catal4020116>
- [18] Wu, Z., Ran, R., Ma, Y., Wu, X., Si, Z., & Weng, D. (2018). Quantitative control and identification of copper species in Cu-SAPO-34: A combined UV-Vis spectroscopic and H₂-TPR analysis. *Research on Chemical Intermediates*, 45(3), 1309–1325. <https://doi.org/10.1007/s11164-018-3680-x>
- [19] Duan, P., & Savage, P. E. (2010). Hydrothermal liquefaction of a microalga with heterogeneous catalysts. *Industrial & Engineering Chemistry Research*, 50(1), 52–61. <https://doi.org/10.1021/ie100758s>
- [20] Ma, C., Geng, J., Zhang, D., & Ning, X. (2020). Hydrothermal liquefaction of macroalgae: Influence of zeolites-based catalyst on products. *Journal of the Energy Institute*, 93(2), 581–590. <https://doi.org/10.1016/j.joei.2019.06.007>
- [21] Wang, H., Tian, W., Zeng, F., Du, H., Zhang, J., & Li, X. (2020). Catalytic hydrothermal liquefaction of spirulina over bifunctional catalyst to produce high-quality biofuel. *Fuel*, 282, 118807. <https://doi.org/10.1016/j.fuel.2020.118807>
- [22] Zhang, B., Lin, Q., Zhang, Q., Wu, K., Pu, W., Yang, M., & Wu, Y. (2017). Catalytic hydrothermal liquefaction of Euglena sp. microalgae over zeolite catalysts for the production of bio-oil. *RSC Advances*, 7(15), 8944–8951. <https://doi.org/10.1039/c6ra28747f>
- [23] Kotelev, M., Tiunov, I., Ivanov, E., & Namsaraev, Z. (2018). Hydrothermal liquefaction-isomerization of biomass for biofuel production. *IOP Conf. Ser.: Earth Environ. Sci.*, 337, 012011. <https://doi.org/10.1088/1755-1315/337/1/012011>
- [24] Wang, A., Chen, Y., Walter, E. D., Washton, N. M., Mei, D., Varga, T., Wang, Y., Szanyi, J., Wang, Y., Peden, C. H. F., & Gao, F. (2019). Unraveling the mysterious failure of Cu/SAPO-34 selective catalytic reduction catalysts. *Nat Commun*, 10, 1137. <https://doi.org/10.1038/s41467-019-09021-3>
- [25] Woo, J., Leistner, K., Bernin, D., Ahari, H., Shost, M., Zammit, M., & Olsson, L. (2018). Effect of various structure directing agents (SDAs) on low-temperature deactivation of Cu/SAPO-34 during NH₃-SCR reaction. *Catalysis Science & Technology*, 8(12), 3090–3106. <https://doi.org/10.1039/c8cy00147b>
- [26] Xu, J., Dong, X., & Wang, Y. (2020). Hydrothermal liquefaction of macroalgae over various solids, basic or acidic oxides and metal salt catalyst: Products distribution and characterization. *Industrial Crops and Products*, 151, 112458. <https://doi.org/10.1016/j.indcrop.2020.112458>
- [27] Li, Y., Zhu, C., Jiang, J., Yang, Z., Feng, W., Li, L., Guo, Y., & Chen, G. (2020). Hydrothermal liquefaction of macroalgae with in-situ-hydrogen donor formic acid: Effects of process parameters on products yield and characterizations. *Industrial Crops and Products*, 153, 112513. <https://doi.org/10.1016/j.indcrop.2020.112513>
- [28] Reddy, H. K., Muppaneni, T., Rastegary, J., Shirazi, S. A., Ghassemi, A., & Deng, S. (2013). ASI: Hydrothermal extraction and characterization of bio-crude oils from wet *Chlorella sorokiniana* and *Dunaliella tertiolecta*. *Environmental Progress & Sustainable Energy*, 32(4), 910–915. <https://doi.org/10.1002/ep.11862>
- [29] Carpio, R. B., Zhang, Y., Kuo, C. T., Chen, W., Schideman, L., & De Leon, R. (2021). Effects of reaction temperature and reaction time on the hydrothermal liquefaction of demineralized wastewater algal biomass. *Bioresource Technology Reports*, 14, 100679. <https://doi.org/10.1016/j.biteb.2021.100679>
- [30] Li, D., Chen, L., Xu, D., Zhang, X., Ye, N., Chen, F., & Chen, S. (2012). Preparation and characteristics of bio-oil from the marine brown alga *Sargassum patens* C. Agardh. *Bioresource Technology*, 104, 737–742. <https://doi.org/10.1016/j.biortech.2011.11.011>
- [31] Hong, C., Wang, Z., Si, Y., Xing, Y., Yang, J., Li, F., Wang, Y., Hu, J., Li, Z., & Li, Y. (2021). Catalytic hydrothermal liquefaction of penicillin residue for the production of bio-oil over different homogeneous/heterogeneous catalysts. *Catalysts*, 11(7), 849. <https://doi.org/10.3390/catal11070849>
- [32] Yeh, T. M., Dickinson, J. G., Franck, A., Linic, S., Thompson, L. T., & Savage, P. E. (2012). Hydrothermal catalytic production of fuels and chemicals from aquatic biomass. *Journal of Chemical Technology and Biotechnology*, 88(1), 13–24. <https://doi.org/10.1002/jctb.3933>

[33] Saber, M. J., Golzary, A., Hosseinpour, M., Takahashi, F., & Yoshikawa, K. (2016). Catalytic hydrothermal liquefaction of microalgae using nanocatalyst. *Applied Energy*, 183, 566–576. <https://doi.org/10.1016/j.apenergy.2016.09.017>

Appendix

Table A.1. Effect of reaction parameter of Hydrothermal Liquefaction of *Nannochloropsis oculata* using ZSM-5 catalyst

Yield (%)	Temperature (°C)			Duration (min.)			Catalyst loading (wt.%)		
	160	200	240	60	90	120	1	3	5
Bio-oil	42.1	58.04	59.16	58.04	54.14	54.14	55.82	58.87	58.04
Solid Residue	54.85	39.75	22.39	39.75	40.98	40.88	34.73	37.62	39.75
Conversion	45.15	60.25	77.61	60.25	59.02	59.12	65.27	62.28	60.25

Control parameter was set at 200 °C; 60 min; 5 wt.%.

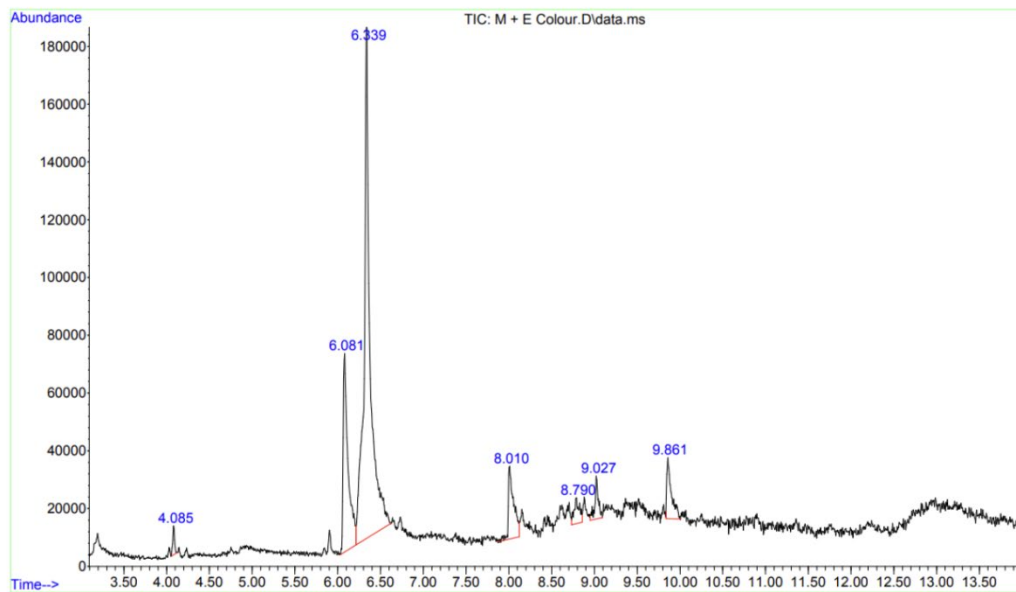


Figure A.2. – GC-MS chromatogram of bio-oil obtained from catalytic screening with catalyst (ZSM-5)

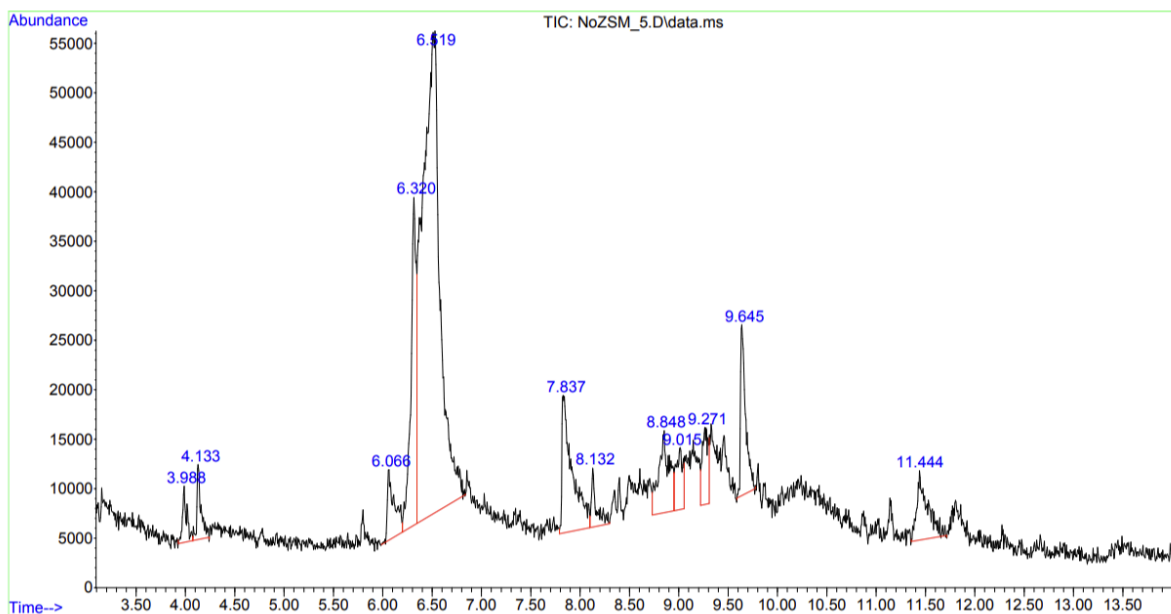


Figure A.3. – GC-MS chromatogram of bio-oil obtained from catalytic screening without catalyst